
The Lie of the Average: How Class Incremental Learning Evaluation Deceives You?

Guannan Lai^{1,2}, Da-Wei Zhou^{1,2}, Xin Yang³, and Han-Jia Ye^{*1,2}

¹School of Artificial Intelligence, Nanjing University

²National Key Laboratory for Novel Software Technology, Nanjing University

³School of Computing and Artificial Intelligence, Southwestern University of Finance and Economics

Email: {laign, zhoudw, yehj}@lamda.nju.edu.cn, yangxin@swufe.edu.cn

Abstract

Class Incremental Learning (CIL) requires models to continuously learn new classes without forgetting previously learned ones, while maintaining stable performance across all possible class sequences. In real-world settings, the order in which classes arrive is diverse and unpredictable, and model performance can vary substantially across different sequences. Yet mainstream evaluation protocols calculate mean and variance from only a small set of randomly sampled sequences. Our theoretical analysis and empirical results demonstrate that this sampling strategy fails to capture the full performance range, resulting in biased mean estimates and a severe underestimation of the true variance in the performance distribution. We therefore contend that a robust CIL evaluation protocol should accurately characterize and estimate the entire performance distribution. To this end, we introduce the concept of extreme sequences and provide theoretical justification for their crucial role in the reliable evaluation of CIL. Moreover, we observe a consistent positive correlation between inter-task similarity and model performance, a relation that can be leveraged to guide the search for extreme sequences. Building on these insights, we propose **EDGE** (Extreme case-based Distribution & Generalization Evaluation), an evaluation protocol that adaptively identifies and samples extreme class sequences using inter-task similarity, offering a closer approximation of the ground-truth performance distribution. Extensive experiments demonstrate that EDGE effectively captures performance extremes and yields more accurate estimates of distributional boundaries, providing actionable insights for model selection and robustness checking. Our code is available at <https://github.com/AIGNLAI/EDGE>.

1 Introduction

Class Incremental Learning (CIL) seeks to equip a model with the ability to incorporate new class knowledge over time while preserving accurate recall of previously learned classes [53, 54]. While much of the literature has centered on advancing architectures and algorithms, the equally crucial question of **how we evaluate CIL** has received far less attention. Recent studies reveal that final performance in CIL is highly sensitive to the sequence in which new classes arrive [3, 21, 31, 49]. Such sensitivity to class order is particularly problematic in realistic settings (e.g., autonomous driving), where the order of class emergence is inherently uncontrollable. Compounding this challenge, the number of possible sequences grows factorially with the number of classes ($O(N!)$), rendering

^{*}Corresponding author.

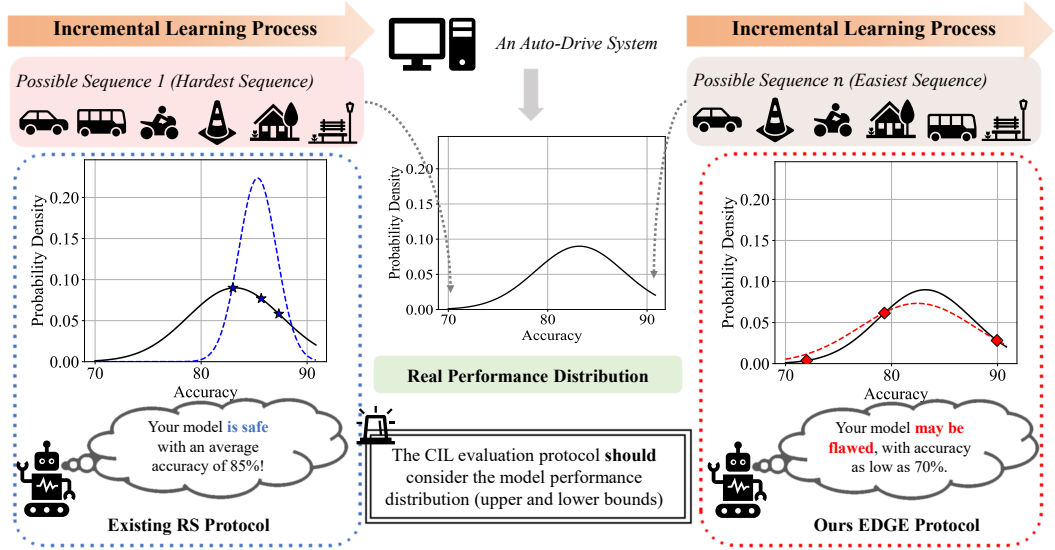


Figure 1: Existing CIL evaluations may be misleading! They merely compute the average accuracy without perceiving the performance distribution, failing to anticipate the impact of potential extreme sequences on the model.

exhaustive evaluation impractical. Consequently, CIL evaluation must rely on sampling only a subset of class sequences to assess and compare model performance.

Existing CIL evaluation protocols [44, 54] typically compute model capability by sampling only 3-5 random class sequences and reporting the sample mean and standard deviation — an approach we call the **Random Sampling (RS) protocol**. Because RS relies on only a handful of sequences, it yields only point estimates and provides no characterization of the full performance distribution. To examine whether RS can reliably approximate the true performance distribution, we conduct a controlled study with **6** classes organized into **3** sequential tasks, resulting in **90** possible class-arrival orders. We exhaustively evaluate each sequence to obtain the ground-truth distribution of test accuracies. Figure 1 illustrates this experimental setting. Consider a realistic incremental-training scenario, such as an autonomous driving system, where numerous intrinsically different class-arrival sequences may occur in practice. Evaluating all sequences in our controlled study produces the ground-truth performance distribution. Analysis of this distribution reveals two key observations: first, the model performance approximately follows a Gaussian shape; second, there is substantial variation in extreme cases, with the gap between the easiest and hardest sequences reaching up to **20%** in our example (Hide-Prompt [39] on CIFAR-100 [15]).

Following the RS protocol, we emulate typical practice by randomly sampling three sequences and fitting a Gaussian $\mathcal{N}(\mu, \sigma^2)$ using their sample mean and variance. As highlighted in the blue box of Figure 1, comparing this RS-estimated Gaussian against the ground-truth distribution reveals systematic bias: RS tends to *overestimate the mean, dramatically underestimate the variance*, and fails to capture the true upper and lower performance bounds. Consequently, selecting models based solely on the reported average is risky — a model with an inflated mean but a poor lower bound may cause severe failures in real-world deployment. These observations demonstrate that RS is inadequate for faithfully capturing CIL performance; a reliable evaluation protocol must either characterize distributional extremes or otherwise provide a substantially better approximation of the full performance distribution.

Motivated by the RS protocol’s neglect of extreme sequences and supported by our theoretical analysis of these cases, we adopt extreme case sampling to more comprehensively characterize model capability and achieve more accurate performance estimates. Through both theoretical and empirical analysis of inter-task similarity and model performance, we identify inter-task similarity as a key factor influencing CIL performance. Building on this insight, we propose **EDGE** (*Extreme case-based Distribution & Generalization Evaluation*), a novel evaluation framework for CIL. EDGE encodes class-level textual descriptions using a pre-trained CLIP model to construct a class similarity matrix. It then generates three representative class sequences: one that maximizes inter-task similarity to simulate an *easy* scenario, one that minimizes it to represent a *difficult* scenario, and one randomly sampled to serve as a *medium* case. Model performance is evaluated on these three sequences,

and their results are aggregated by computing the mean and standard deviation, providing a more comprehensive approximation of the model’s performance distribution. As highlighted in the red box of Figure 1, EDGE produces a substantially closer approximation to the ground-truth distribution than the RS protocol, capturing both the central tendency and the distributional extremes.

The main contributions of this work are summarized as follows:

- We conduct a systematic study of evaluation protocols in CIL, emphasizing that evaluation should aim to capture the full performance distribution of a model. Through both theoretical analysis and empirical investigation, we show that the widely adopted RS protocol produces biased estimates and fails to reflect the realistic behavior of CIL models.
- We propose **EDGE** (*Extreme case-based Distribution & Generalization Evaluation*), a novel evaluation framework that adaptively identifies and samples both easy and challenging class sequences based on inter-task similarity, thereby providing a more faithful approximation of the ground-truth performance distribution.
- Extensive experiments validate the effectiveness of EDGE in sampling extreme sequences and estimating model performance accurately. Our analysis also uncovers notable phenomena, such as different methods exhibiting comparable lower-bound performance in specific scenarios, offering critical insights for the design of future CIL models.

2 Related Work

Class Incremental Learning (CIL): Existing CIL approaches can be broadly categorized into non-pre-trained and pre-trained based methods [4, 9]. Non-pre-trained methods typically fall into three categories: (1) Regularization-based methods, which introduce explicit regularization terms into the loss function to balance the learning dynamics between old and new tasks [1, 14, 20, 46]; (2) Replay-based methods, which alleviate catastrophic forgetting by replaying data from past tasks, either through stored exemplars [6, 23, 30, 38] or via generative samples synthesized by GANs [8, 22, 32, 58]; and (3) Dynamic network methods, which modify the network architecture—such as by expanding layers or neurons—to accommodate new knowledge while preserving prior information [2, 5, 27, 42, 43]. In contrast, PTM-based methods leverage the representational power of pre-trained backbones and mitigate forgetting through three main strategies: (1) Prompt-based methods, which apply lightweight updates via prompt tuning while freezing the backbone to maintain generalization [13, 19, 33, 40, 47, 48]; (2) Model mixture-based methods, which store intermediate checkpoints and integrate them using ensemble or model-merging techniques [11, 41, 45, 52, 55, 57]; and (3) Prototype-based methods, which classify examples using nearest-class-mean strategies grounded in PTM-derived embeddings [16, 24, 28, 53].

Evaluation Protocols of CIL: Evaluation protocols in CIL have received comparatively limited attention. Prior studies such as [10, 12, 25] propose multi-dimensional assessment criteria and benchmarks, while [7] investigates dynamic task allocation to probe lower-bound performance. In contrast, our work adopts a distribution-oriented perspective: rather than relying on a few random trials, we aim to estimate the underlying performance distribution via a small set of informative, extreme-aware samples. This approach enables more reliable assessment under atypical or adversarial class sequences and delivers more actionable guidance for model selection and design.

3 Preliminaries

3.1 Problem Definition

Class Incremental Learning (CIL). Given an ordered sequence of tasks $\{1, \dots, t, \dots\}$, each task i is associated with a training set $\mathcal{D}^i = \{X^i, Y^i\}$, where X^i denotes the input samples and Y^i the corresponding labels. Let CLS^i denote the class set for task i , with cardinality $|CLS^i|$. A crucial constraint enforces strict separation between tasks: $\forall i \neq j \in \{1, \dots, n\}$, $CLS^i \cap CLS^j = \emptyset$, and no inter-task data accessibility is allowed during training. The goal of CIL is to learn a unified embedding function $\Psi : \mathcal{D}^i \rightarrow \mathbb{R}^d$ that maps inputs to a shared embedding space, along with a classifier $f(\cdot)$ capable of maintaining discriminative performance across all encountered tasks.

In the CIL scenario, given a sequence of learning classes \mathcal{O} comprising T tasks, we define $A_{t,t'}$ as the classification accuracy of the model on the test set of the t' -th task after training on the first t

tasks. Based on this, the overall evaluation metric for sequence \mathcal{O} can be formally defined as:

$$\mathcal{A}(\mathcal{O}) = \frac{1}{T} \sum_{t=1}^T A_{T,t}. \quad (1)$$

Objective of CIL Evaluation Protocol Design. Let Ω denote the space of all possible class sequences under a given CIL setting. By sampling L sequences $\{\mathcal{O}_1, \dots, \mathcal{O}_L\} \subset \Omega$ and computing their final accuracies $\mathcal{A}(\mathcal{O}_l)$ using Equation (1), we construct an empirical performance distribution \mathcal{P}_{emp} with mean $\mu_{\mathcal{A}}$ and standard deviation $\sigma_{\mathcal{A}}$.

As shown in Figure 1 and the *appendix*, the realistic distribution $\mathcal{P}_{\text{true}}$ is approximately Gaussian. We therefore use $\mathcal{N}(\mu_{\mathcal{A}}, \sigma_{\mathcal{A}}^2)$ to approximate it, and define the goal of protocol design as minimizing the distributional distance between $\mathcal{P}_{\text{true}}$ and its estimate, measured by metrics such as Jensen-Shannon divergence [17] or Wasserstein distance [36].

Random Sampling (RS) Evaluation Protocol. For a given CIL model \mathcal{M} , the conventional evaluation protocol uses three fixed random seeds [16, 18, 24, 48] to generate class sequences $\{RS_l\}_{l=1}^3$. The performance of the model is then estimated by computing the mean and standard deviation of final accuracies: $\mu_{\mathcal{A}} = \frac{1}{3} \sum_{l=1}^3 \mathcal{A}(RS_l)$, $\sigma_{\mathcal{A}}^2 = \frac{1}{3} \sum_{l=1}^3 (\mathcal{A}(RS_l) - \mu_{\mathcal{A}})^2$. However, prior work only uses these statistics to summarize performance, without evaluating how well the estimated distribution matches the true one. This leads to overconfidence in the evaluation results and may result in misleading conclusions.

3.2 Limitations of RS Evaluation Protocol

Despite the substantial advances in CIL, to our knowledge, no prior work has critically examined the validity of prevailing evaluation protocols. In this section, we undertake theoretical investigations to address this oversight. *All theoretical results and proofs in this section are provided in the Appendix.*

First, we demonstrate through Lemma 1 that CIL evaluation cannot be reliably accomplished using existing RS protocols, due to the combinatorial explosion in the number of possible class sequences.

Lemma 1. *Let N be the total number of classes, partitioned into K tasks of equal size $M = N/K$. Then the number of distinct class sequences is $|\Omega| = \frac{N!}{(M!)^K}$. Moreover, under linear scaling $K = \Theta(N)$, the quantity $|\Omega|$ grows factorially, satisfying $|\Omega| = \Omega((N/e)^N)$, which asymptotically dwarfs any polynomial-scale sampling capacity as $N \rightarrow \infty$.*

For $N = 100$ classes divided into $K = 10$ tasks, the number of possible sequences is approximately 10^{92} , vastly exceeding practical enumeration. The RS protocols typically sample only 3 class sequences, covering less than $10^{-90}\%$ of the space and thus suffering from severe under-sampling bias. Building on Lemma 1, we now ask: **How Many** random sequence samples are required to approximate the true accuracy distribution over the full sequence space within a given tolerance?

Theorem 1. *Let Ω be the set of all possible class sequences with $|\Omega|$ elements, and fix tolerance $\varepsilon > 0$ and failure probability $\delta \in (0, 1)$. Suppose we draw L sequences $\{RS_l\}_{l=1}^L$ without replacement uniformly from Ω , and let $\hat{\mathcal{A}}_L = \frac{1}{L} \sum_{l=1}^L \mathcal{A}(RS_l)$ be the empirical mean, respectively. Then for any $\varepsilon > 0$, if*

$$L \frac{|\Omega| - L}{|\Omega| - 1} \geq \frac{\ln(2|\Omega|/\delta)}{2\varepsilon^2}, \quad (2)$$

then with probability at least $1 - \delta$, $|\hat{\mathcal{A}}_L - \mathbb{E}_{\omega}[\mathcal{A}(\omega)]| \leq \varepsilon$.

Remark 1. *Substituting $|\Omega| = N!/(M!)^K \approx (N/e)^N$ from Lemma 1, the condition (2) becomes*

$$L \frac{\frac{N!}{(M!)^K} - L}{\frac{N!}{(M!)^K} - 1} \geq \frac{\ln(2/\delta) + \ln(N!/(M!)^K)}{2\varepsilon^2} \approx \frac{1}{2\varepsilon^2} \left[N \ln(N/e) + \ln \frac{2}{\delta} \right]. \quad (3)$$

For large $|\Omega|$ and $L \ll |\Omega|$, the finite-population correction $\frac{|\Omega| - L}{|\Omega| - 1} \approx 1$, so one recovers the same sample complexity scale $\Omega(\frac{N \ln N}{\varepsilon^2})$ as in the with-replacement case. Even for moderate N (e.g. $N = 100$) and a coarse $\varepsilon = 0.1$, achieving high confidence (say $\delta = 0.05$) still requires on the order of $L \gtrsim 2 \times 10^4$ samples, so purely random sampling remains fundamentally impractical.

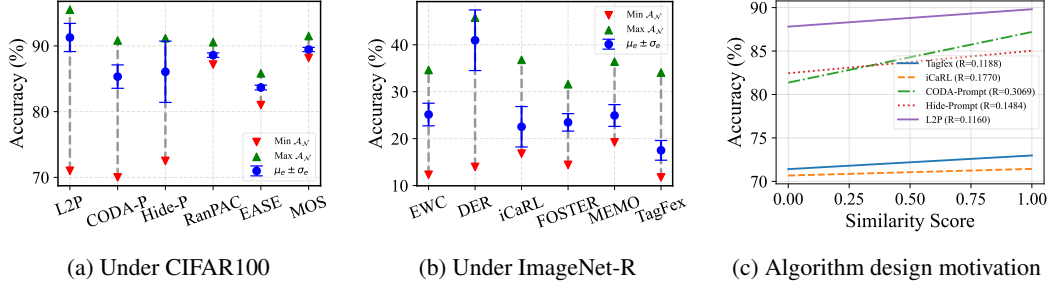


Figure 2: Figures 2a and 2b show model performance under fully enumerable scenarios (green: maximum, red: minimum), along with estimates from the random sampling (RS) protocol (blue error bars). Figure 2c illustrates the correlation between inter-task similarity scores and model performance, where R denotes the Pearson correlation coefficient.

Noting that in Equation (3) we have $L \ll |\Omega|$, let $E_t = \{\omega \in \Omega : |\mathcal{A}(\omega) - \mathbb{E}_\omega[\mathcal{A}(\omega)]| > t \sqrt{\text{Var}_\omega[\mathcal{A}(\omega)]}\}$. The probability that none of the L sampled sequences falls into E_t is approximately $\exp(-(|E_t|/|\Omega|)L)$. Hence, uniform random sampling almost surely fails to capture model performance in the most extreme cases. This observation motivates the idea of deliberately constructing such **extreme class sequences** to directly evaluate easy and hard case performance; Theorem 2 provides an initial theoretical analysis of this approach:

Theorem 2. *Let Ω be the set of all class sequences, and define $\mu = \mathbb{E}_{\omega \sim \Omega}[\mathcal{A}(\omega)]$, $\sigma = \sqrt{\text{Var}_{\omega \sim \Omega}[\mathcal{A}(\omega)]}$ as the realistic mean and standard deviation of the accuracy function \mathcal{A} . Suppose we know two extreme sequences ω_+ , ω_- satisfying $\mathcal{A}(\omega_+) - \mu \geq \sigma$ and $\mu - \mathcal{A}(\omega_-) \geq \sigma$. Draw L sequences $\{RS_l\}_{l=1}^L$ without replacement uniformly from $\Omega \setminus \{\omega_+, \omega_-\}$, and define $\tilde{\mathcal{A}}_{L+2} = \frac{1}{L+2} \left[\mathcal{A}(\omega_-) + \mathcal{A}(\omega_+) + \sum_{l=1}^L \mathcal{A}(RS_l) \right]$. Then for any $\varepsilon > 0$ and $\delta \in (0, 1)$, if*

$$L \frac{|\Omega| - 2 - L}{|\Omega| - 3} \geq \frac{\ln(2(|\Omega| - 2)/\delta) (R^{(\sigma)})^2}{2\varepsilon^2}, \quad (4)$$

where $R^{(\sigma)} = \mathcal{A}(\omega_+) - \mathcal{A}(\omega_-)$, then with probability at least $1 - \delta$, $|\tilde{\mathcal{A}}_{L+2} - \mathbb{E}_{\omega \sim \Omega}[\mathcal{A}(\omega)]| \leq \varepsilon$.

Remark 2. *Theorem 2 demonstrates that, under the conditions outlined in Remark 1, incorporating extreme class sequences reduces the required sample size to a value proportional to $(R^{(\sigma)})^2$. For instance, when $R^{(\sigma)} \approx 0.1$ (which is common in practical scenarios), the lower bound on the sample size L drops to around 50. This represents a significant reduction compared to uniform random sampling, underscoring the practical benefit of extreme-sequence-assisted evaluation in CIL.*

4 EDGE: Extreme case-based Distribution & Generalization Evaluation

4.1 Motivation

Building on the theoretical analyses in Section 3.2, we conduct an exhaustive evaluation under a 6-class, 3-task setting. As illustrated in Figures 2a and 2b, the RS protocol often fails to accurately estimate the true performance distribution, frequently leading to either underestimation or overestimation of certain models, which compromises fairness in comparison. Meanwhile, the findings from Theorem 2, together with the **near-Gaussian** nature of the true distribution, highlight the importance of incorporating extreme class sequences to improve evaluation quality. Nevertheless, a key challenge remains in how to effectively leverage dataset-specific structures and characteristics to generate extreme sequences that are both robust and generalizable, thereby enabling more reliable and informative evaluation protocols.

In the CIL setting, it is intuitively understood that when adjacent tasks exhibit low similarity, model parameters undergo significant changes during task transitions, which increases the risk of forgetting. To investigate this phenomenon further, we examine the relationship between inter-task similarity and model generalization error.

Theorem 3. *Consider a CIL system consisting of K tasks, where each task T_k is associated with a data distribution \mathcal{D}_k and a class set \mathcal{C}_k . The generalization error is defined as $\epsilon_g =$*

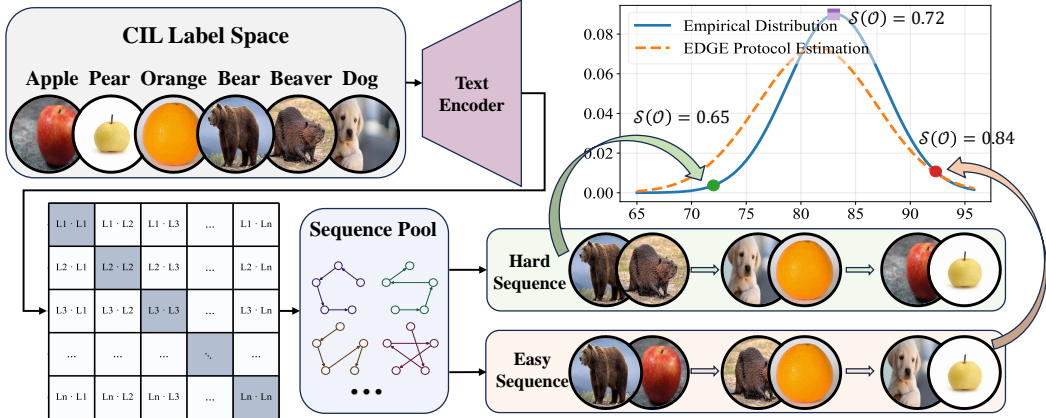


Figure 3: Illustration of the EDGE evaluation protocol. The sequence with a green background represents a hard case, where similar classes (e.g., apples and pears) appear within the same task, resulting in low inter-task similarity. The sequence with an orange background represents an easy case, where similar classes are distributed across different tasks, leading to high inter-task similarity.

$\frac{1}{K} \sum_{k=1}^K \mathbb{E}_{(x,y) \sim \mathcal{D}_k} [L(h(x), y)]$, where $L(h(x), y)$ denotes the loss between the model prediction $h(x)$ and the true label y . Given a task order $\mathcal{O} = \{T_1, T_2, \dots, T_K\}$, the similarity score $S(\mathcal{O})$ is defined as:

$$S(\mathcal{O}) = \frac{K}{(K-1)N} \sum_{1 \leq i \leq K-1} \sum_{c \in \mathcal{C}_i} \sum_{c' \in \mathcal{C}_{i+1}} \text{Sim}(c, c'), \quad (5)$$

where $\text{Sim}(c, c')$ denotes the semantic similarity in the representation space between classes c and c' , belonging to tasks T_i and T_j , respectively. Let \mathcal{O}_h and \mathcal{O}_e denote the sequences with the minimum and maximum similarity scores $S(\mathcal{O})$, respectively, and let \mathcal{O}_r represent a randomly generated sequence. Then, the following conditions hold:

- The similarity score satisfies $S(\mathcal{O}_h) \leq S(\mathcal{O}_r) \leq S(\mathcal{O}_e)$,
- The generalization error satisfy $\epsilon_g(\mathcal{O}_h) \geq \epsilon_g(\mathcal{O}_r) \geq \epsilon_g(\mathcal{O}_e)$.

Theorem 3 theoretically demonstrates that as task similarity decreases, the upper bound of the generalization error increases significantly. Figure 2c illustrates the trend between inter-task similarity scores and corresponding model performance for all possible class sequences. The majority of methods show a positive correlation, empirically supporting this result by showing a consistent decline in model accuracy as task similarity decreases. Motivated by these observations, we take advantage of inter-task similarity to construct extreme class sequences, which facilitates a more thorough and representative evaluation of CIL.

4.2 Extreme Sequence Generation Algorithm and Proposed Protocol

Figure 3 illustrates the proposed EDGE evaluation protocol. Given a dataset, since direct access to image instances is unavailable, we leverage the text encoder from a pre-trained CLIP model to embed class labels. Specifically, each class label is encoded into a d -dimensional semantic feature vector via the CLIP text encoder Φ , forming a label feature set $\mathcal{L} = \{\mathbf{L}_1, \dots, \mathbf{L}_N\}$, where $\mathbf{L}_i = \Phi(y_i) \in \mathbb{R}^d$. By computing cosine similarities between these label features, we construct a symmetric similarity matrix $\mathbf{D} \in \mathbb{R}^{N \times N}$, where each entry $d_{ij} = \frac{\mathbf{L}_i \cdot \mathbf{L}_j}{\|\mathbf{L}_i\| \|\mathbf{L}_j\|}$ quantifies the semantic similarity between classes i and j . Based on the similarity matrix \mathbf{D} , we generate candidate class sequences by hierarchically clustering [26] semantically similar classes and strategically selecting subsequent tasks to minimize or maximize inter-task similarity. Two optimal permutations are identified using Equation (5): $\mathcal{O}_h = \arg \min_{o \in \Omega} S(o)$ for the hardest sequence and $\mathcal{O}_e = \arg \max_{o \in \Omega} S(o)$ for the easiest sequence. To ensure the total number of sampled sequences remains unchanged, we randomly select one sequence as the *Median Sequence*, which is theoretically guaranteed to lie near the center of the distribution Theorem 1. By evaluating models on this triplet of task sequences, we approximate the true performance distribution and enable a more comprehensive assessment of model capability.

Table 1: Experimental results of pre-trained-based methods on two datasets. The gray region indicates the ground-truth values, and the best results are highlighted in bold black.

Metric	CIFAR-100						ImageNet-R					
	L2P	CODA-Prompt	Hide-Prompt	EASE	MOS	RanPAC	L2P	CODA-Prompt	Hide-Prompt	EASE	MOS	RanPAC
$\min_{\mathcal{A}_N}$	71.83	64.67	72.50	95.33	92.17	98.50	57.75	18.72	65.90	88.24	85.56	90.91
RS	83.83	76.83	79.67	95.50	95.33	98.67	68.98	39.04	78.34	88.77	87.17	93.05
EDGE	72.83	73.00	73.00	95.33	93.83	98.67	66.31	21.93	71.89	88.24	86.10	93.05
$\max_{\mathcal{A}_N}$	92.50	87.00	91.17	95.83	97.67	98.83	83.42	57.75	82.95	88.77	91.98	96.26
RS	87.33	81.83	90.67	95.50	95.83	98.83	75.40	43.85	78.34	88.77	87.70	95.19
EDGE	92.00	84.17	90.75	95.67	96.67	98.83	77.54	45.45	76.04	88.77	91.44	95.19
JSD_{RS}	0.44	0.38	0.34	0.00	0.15	0.00	0.23	0.65	0.41	0.00	0.37	0.57
JSD_{EDGE}	0.30	0.28	0.22	0.00	0.15	0.00	0.21	0.20	0.18	0.00	0.17	0.36
W_{RS}	2.81	2.92	3.89	0.00	0.48	0.00	1.59	9.85	2.44	0.00	1.18	2.25
W_{EDGE}	2.00	2.03	1.42	0.00	0.22	0.00	1.74	2.37	1.11	0.00	0.77	1.07

To generate hard sequences, we first cluster classes based on semantic similarity using hierarchical clustering [26]. To encourage semantically similar classes to be grouped into the same task, we preserve large clusters intact and selectively split smaller ones as needed, ensuring all classes are assigned to K tasks while minimizing global inter-task similarity.

After constructing task partitions, we compute the inter-task similarity matrix $\mathbf{ITS} \in \mathbb{R}^{K \times K}$ and initialize the sequence with the task exhibiting the lowest global similarity. Subsequent tasks are iteratively selected based on minimal similarity to the current task, forming candidate sequences.

By varying the clustering granularity, we generate multiple candidates and select the one with the lowest overall similarity score $\mathcal{S}(o)$. The easy sequence is constructed analogously, except that similar classes are intentionally assigned to different tasks, and each next task is selected based on maximal similarity to the previous one. *Pseudo-code and analysis are provided in the Appendix.*

5 Experiment

Due to the exponential growth in the number of possible class sequences in CIL scenarios (as shown in Lemma 1), obtaining the true performance distribution under standard experimental settings is infeasible. We therefore divide our experimental evaluation into two parts. First, we conduct **fully enumerable** experiments on subsets of standard datasets, enabling quantitative analysis to validate the effectiveness of the proposed EDGE protocol. Second, we perform analytical experiments under standard benchmark settings, visually demonstrating EDGE’s strong capability in capturing extreme performance cases.

5.1 Enumerable Experiments

5.1.1 Experimental Setup

Dataset and Metrics. We conduct experiments on the CIFAR-100 and ImageNet-R [15] datasets. For each dataset, we select the first six classes and partition them into three tasks, generating 90 possible task permutations, which we consider the true distribution (\mathcal{D}_{true}). Next, we apply the RS evaluation protocol (using random seeds 0, 42, and 1993 [16, 18, 24, 48]) to generate class sequences for evaluation, obtaining the estimated distribution \mathcal{D}_{RS} . Simultaneously, we employ the EDGE protocol to perform the evaluation, yielding the estimated distribution \mathcal{D}_{EDGE} . To quantitatively assess the effectiveness of different evaluation strategies, we use the JSD divergence and Wasserstein distance (JSD_d [17] and W_d [36]) to measure the differences between the estimated and true distributions.

Baseline. To ensure a fair comparison, we benchmark our method under both non-pre-trained and pre-trained settings against classic and state-of-the-art approaches: in the non-pre-trained setting, we compare with EWC [14], DER [50], iCaRL [29], FOSTER [38], MEMO [56], and TagFex [51]; in the pre-trained setting, following Sun et al. [34], we evaluate against L2P [48], CODA-Prompt [33], HidePrompt [39], EASE [55], and MOS [35].

Implementation Details. Our framework is implemented in PyTorch, and the code is provided in the *supplementary materials*. Complete experimental details can be found in the *appendix*.

Table 2: Experimental results of non-pre-trained-based methods on two datasets. Details are consistent with those in Table 1.

Metric	CIFAR-100					ImageNet-R					
	EWC	DER	iCaRL	FOSTER	MEMO	EWC	DER	iCaRL	FOSTER	MEMO	TagFex
$\text{min}_{\mathcal{A}_N}$	12.50	16.83	36.33	16.00	21.83	10.06	11.73	10.61	11.17	12.85	11.73
RS	26.17	24.17	43.00	20.67	36.50	16.76	11.73	14.53	15.08	15.05	18.99
EDGE	12.50	26.35	38.50	16.67	35.67	10.61	11.97	14.53	11.73	15.44	14.53
$\text{max}_{\mathcal{A}_N}$	39.00	45.50	53.33	38.33	56.67	27.93	26.26	43.58	26.82	30.73	21.23
RS	27.50	34.17	43.00	23.50	51.17	21.23	18.99	22.91	24.02	21.23	20.11
EDGE	28.17	41.33	43.33	30.17	56.67	24.58	21.23	26.82	23.95	28.49	20.67
JSD_{RS}	0.51	0.29	0.36	0.58	0.29	0.36	0.32	0.30	0.22	0.38	0.44
JSD_{EDGE}	0.29	0.31	0.32	0.40	0.23	0.26	0.20	0.21	0.20	0.16	0.15
W_{RS}	4.74	4.62	2.37	6.25	2.00	2.40	2.14	3.14	2.11	2.99	3.14
W_{EDGE}	3.44	3.22	2.03	3.91	1.82	2.03	1.07	2.71	1.03	1.66	0.88

5.1.2 Experiment Results

Tables 1 and 2 present the experimental results of two types of methods on the CIFAR-100 and ImageNet-R datasets. The results are organized into four sections: the first section shows the true lower performance bound (highlighted in gray) along with the lower bounds estimated by RS and EDGE; the second section similarly compares the upper performance bounds. The third and fourth sections display the JSD Divergence and the Wasserstein Distance, respectively, between the estimated distributions from both methods and the true distribution. Based on these experimental results, we draw the following conclusions:

- **RS leads to inaccurate and unfair comparisons.** RS produces biased estimates of performance boundaries, which may lead to unfair comparisons among models. For example, when evaluating non-pre-trained methods on the CIFAR-100 dataset, the lower bound estimated by RS for EWC (26.17%) is significantly higher than its true lower bound (12.50%). Notably, although the true lower bound of DER (16.83%) is actually better than that of EWC, the RS estimate suggests a worse lower bound for DER (24.17%), leading to an erroneous conclusion. In contrast, EDGE provides more accurate estimations of these boundaries, thereby avoiding such incorrect comparisons.
- **EDGE captures extremes and supports more comprehensive evaluation.** In the vast majority of experimental cases, the performance bounds estimated by EDGE are significantly closer to the ground-truth bounds (gray area) than those estimated by RS. Furthermore, EDGE demonstrates a stronger capability in approximating the true performance distribution, as reflected in its consistently lower or equal JSD Divergence and Wasserstein Distance values compared to RS in most scenarios.
- **Multiple methods may converge to similar worst-case performance under hard sequences.** On the challenging ImageNet-R dataset, the true lower-bound performance (i.e., worst-case accuracy) of multiple non-pre-trained methods clusters within a narrow range of 10.06% to 12.85%. This consistency suggests that task difficulty itself, rather than architectural differences, constitutes the primary bottleneck in this setting. EDGE helps model developers recognize this phenomenon, highlighting that variations in model design have limited impact under such conditions.
- **The accuracy of boundary estimation is correlated with model performance stability.** A model’s performance stability directly affects how accurately its bounds can be estimated. Models with stable performance and low variance (e.g., EASE, MOS, and RanPAC in Table 1) enable both RS and EDGE to estimate bounds accurately, yielding near-zero JSD and Wasserstein Distance. In contrast, models with high performance fluctuation (e.g., non-pre-trained methods in Table 2) pose greater challenges for bound estimation. It is in these cases that EDGE shows a clearer advantage over RS, producing closer bound estimates and lower distribution distances.

EDGE is robust across different configurations. Figure 4 demonstrates that the EDGE protocol maintains high estimation accuracy under various settings, including different model backbones (e.g., ResNet vs. ViT) and different sizes of the CLIP text encoder. In all cases, EDGE consistently outperforms the RS protocol by providing estimates that more closely align with the ground-truth performance distribution. This highlights the reliability and generalizability of EDGE across diverse model architectures and embedding capacities. *Additional results and detailed analyses for other experimental settings are provided in the appendix.*

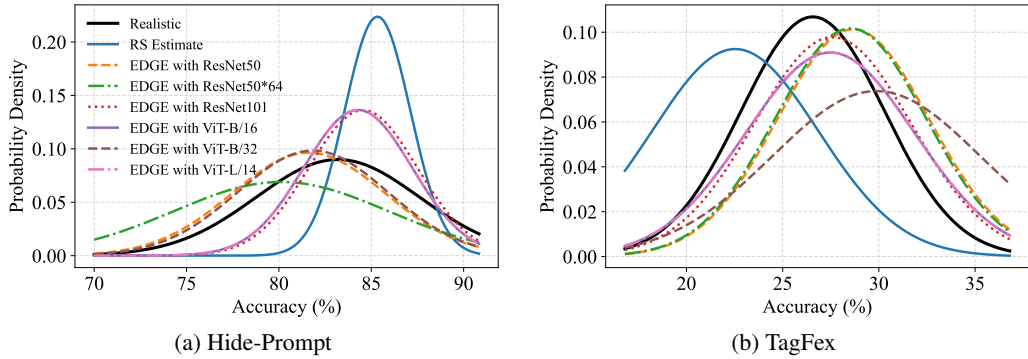


Figure 4: Effect of task sequences generated with CLIP text encoders of varying scales on the estimation of performance distributions under the EDGE protocol. The black curve denotes the ground-truth distribution, and the blue curve indicates the estimation obtained via the RS protocol.

5.2 Experiments on Classic CIL Settings

Following the classic CIL setup, we conduct experiments using three datasets: CIFAR-100 [15], CUB-200 [37], ImageNet-R [15]. Each dataset is partitioned into multiple tasks of equal size. Figure 5 visualizes the maximum and minimum accuracy values ($\max_{\mathcal{A}}$ and $\min_{\mathcal{A}}$) of the sampled sequences under each protocol, highlighting their ability to capture the extremes of the performance distribution. The results demonstrate that EDGE consistently achieves both a lower estimated lower bound and a higher upper bound across nearly all scenarios, including highly stable methods such as EASE [55] and RanPAC [24]. This allows it to identify rare but critical performance extremes, providing a more reliable and practical assessment of performance for real-world deployments. *For more detailed analysis, please refer to the Appendix.*

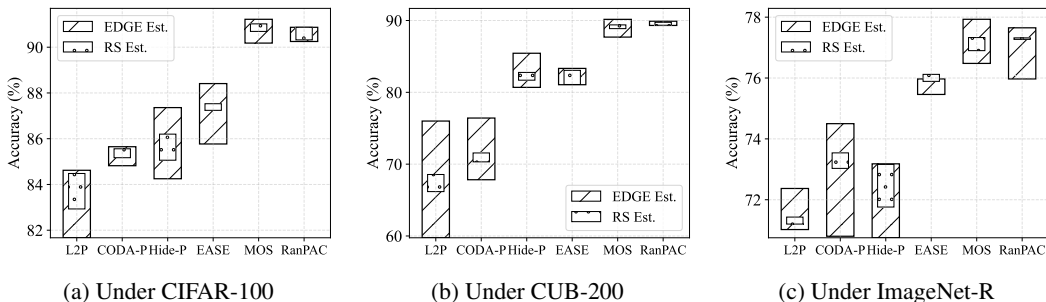


Figure 5: Visualization of the estimated lower and upper performance bounds across three datasets under the classic CIL setting: (a) CIFAR-100, (b) CUB-200, and (c) ImageNet-R. The slashed bars (/) denote the proposed **EDGE**, while the dotted bars (.) correspond to the existing **RS** protocol.

6 Conclusions and Discussion

This paper introduces a new perspective on evaluating CIL, highlighting the theoretical and empirical limitations of conventional RS protocols. We propose EDGE, an evaluation protocol that adaptively constructs task sequences with varying difficulty levels based on inter-task similarity, enabling a more accurate and comprehensive assessment of model performance.

References

- [1] Rahaf Aljundi, Francesca Babiloni, Mohamed Elhoseiny, Marcus Rohrbach, and Tinne Tuytelaars. Memory aware synapses: Learning what (not) to forget. In *ECCV*, 2018.
- [2] Rahaf Aljundi, Punarjay Chakravarty, and Tinne Tuytelaars. Expert gate: Lifelong learning with a network of experts. In *CVPR*, 2017.

- [3] Samuel J Bell and Neil D Lawrence. The effect of task ordering in continual learning. *arXiv preprint arXiv:2205.13323*, 2022.
- [4] Boxi Cao, Qiaoyu Tang, Hongyu Lin, Xianpei Han, Jiawei Chen, Tianshu Wang, and Le Sun. Retentive or forgetful? diving into the knowledge memorizing mechanism of language models. *arXiv preprint arXiv:2305.09144*, 2023.
- [5] Xuemei Cao, Hanlin Gu, Xin Yang, Bingjun Wei, Haoyang Liang, Xiangkun Wang, and Tianrui Li. Erroreraser: Unlearning data bias for improved continual learning. In *SIGKDD*, 2025.
- [6] Hyuntak Cha, Jaeho Lee, and Jinwoo Shin. Co2l: Contrastive continual learning. In *CVPR*, 2021.
- [7] Shengzhuang Chen, Yikai Liao, Xiaoxiao Sun, Kede Ma, and Ying Wei. Cldyb: Towards dynamic benchmarking for continual learning with pre-trained models. *ICLR*, 2025.
- [8] Yulai Cong, Miaoyun Zhao, Jianqiao Li, Sijia Wang, and Lawrence Carin. Gan memory with no forgetting. *NeurIPS*, 2020.
- [9] Shihbansh Dohare, J Fernando Hernandez-Garcia, Qingfeng Lan, Parash Rahman, A Rupam Mahmood, and Richard S Sutton. Loss of plasticity in deep continual learning. *Nature*, 2024.
- [10] Sebastian Farquhar and Yarin Gal. Towards robust evaluations of continual learning. *arXiv preprint arXiv:1805.09733*, 2018.
- [11] Qiankun Gao, Chen Zhao, Yifan Sun, Teng Xi, Gang Zhang, Bernard Ghanem, and Jian Zhang. A unified continual learning framework with general parameter-efficient tuning. In *ICCV*, 2023.
- [12] Yen-Chang Hsu, Yen-Cheng Liu, Anita Ramasamy, and Zsolt Kira. Re-evaluating continual learning scenarios: A categorization and case for strong baselines. *arXiv preprint arXiv:1810.12488*, 2018.
- [13] Menglin Jia, Luming Tang, Bor-Chun Chen, Claire Cardie, Serge Belongie, Bharath Hariharan, and Ser-Nam Lim. Visual prompt tuning. In *ECCV*, 2022.
- [14] James Kirkpatrick, Razvan Pascanu, Neil Rabinowitz, Joel Veness, Guillaume Desjardins, Andrei A Rusu, Kieran Milan, John Quan, Tiago Ramalho, Agnieszka Grabska-Barwinska, et al. Overcoming catastrophic forgetting in neural networks. *National Academy of Sciences*, 2017.
- [15] A Krizhevsky. Learning multiple layers of features from tiny images. *Master's thesis, University of Tront*, 2009.
- [16] Guannan Lai, Yujie Li, Xiangkun Wang, Junbo Zhang, Tianrui Li, and Xin Yang. Order-robust class incremental learning: Graph-driven dynamic similarity grouping. In *CVPR*, 2025.
- [17] Pedro W Lamberti, Ana P Majtey, Marcos Madrid, and María E Pereyra. Jensen-shannon divergence: A multipurpose distance for statistical and quantum mechanics. In *AIP Conference Proceedings*, 2007.
- [18] Qiwei Li and Jiahuan Zhou. Caprompt: Cyclic prompt aggregation for pre-trained model based class incremental learning. In *AAAI*, 2025.
- [19] Yujie Li, Xin Yang, Hao Wang, Xiangkun Wang, and Tianrui Li. Learning to prompt knowledge transfer for open-world continual learning. In *AAAI*, 2024.
- [20] Zhizhong Li and Derek Hoiem. Learning without forgetting. *TPAMI*, 2017.
- [21] Sen Lin, Peizhong Ju, Yingbin Liang, and Ness Shroff. Theory on forgetting and generalization of continual learning. In *ICML*, 2023.
- [22] Xialei Liu, Chenshen Wu, Mikel Menta, Luis Herranz, Bogdan Raducanu, Andrew D Bagdanov, Shangling Jui, and Joost van de Weijer. Generative feature replay for class-incremental learning. In *CVPR Workshops*, 2020.

[23] David Lopez-Paz and Marc’ Aurelio Ranzato. Gradient episodic memory for continual learning. *NeurIPS*, 2017.

[24] Mark D McDonnell, Dong Gong, Amin Parvaneh, Ehsan Abbasnejad, and Anton van den Hengel. Ranpac: Random projections and pre-trained models for continual learning. *NeurIPS*, 2024.

[25] Martin Mundt, Steven Lang, Quentin Delfosse, and Kristian Kersting. Cleva-compass: A continual learning evaluation assessment compass to promote research transparency and comparability. *arXiv preprint arXiv:2110.03331*, 2021.

[26] Frank Nielsen and Frank Nielsen. Hierarchical clustering. *Introduction to HPC with MPI for Data Science*, 2016.

[27] Oleksiy Ostapenko, Pau Rodriguez, Massimo Caccia, and Laurent Charlin. Continual learning via local module composition. *NeurIPS*, 2021.

[28] Aristeidis Panos, Yuriko Kobe, Daniel Olmeda Reino, Rahaf Aljundi, and Richard E Turner. First session adaptation: A strong replay-free baseline for class-incremental learning. In *ICCV*, 2023.

[29] Sylvestre-Alvise Rebuffi, Alexander Kolesnikov, Georg Sperl, and Christoph H Lampert. icarl: Incremental classifier and representation learning. In *CVPR*, 2017.

[30] Matthew Riemer, Ignacio Cases, Robert Ajemian, Miao Liu, Irina Rish, Yuhai Tu, and Gerald Tesauro. Learning to learn without forgetting by maximizing transfer and minimizing interference. *arXiv preprint arXiv:1810.11910*, 2018.

[31] Haozhe Shan, Qianyi Li, and Haim Sompolinsky. Order parameters and phase transitions of continual learning in deep neural networks. *arXiv preprint arXiv:2407.10315*, 2024.

[32] Hanul Shin, Jung Kwon Lee, Jaehong Kim, and Jiwon Kim. Continual learning with deep generative replay. *NeurIPS*, 2017.

[33] James Seale Smith, Leonid Karlinsky, Vyshnavi Gutta, Paola Cascante-Bonilla, Donghyun Kim, Assaf Arbelle, Rameswar Panda, Rogerio Feris, and Zsolt Kira. Coda-prompt: Continual decomposed attention-based prompting for rehearsal-free continual learning. In *CVPR*, 2023.

[34] Hai-Long Sun, Da-Wei Zhou, De-Chuan Zhan, and Han-Jia Ye. Pilot: A pre-trained model-based continual learning toolbox, 2025.

[35] Hai-Long Sun, Da-Wei Zhou, Hanbin Zhao, Le Gan, De-Chuan Zhan, and Han-Jia Ye. Mos: Model surgery for pre-trained model-based class-incremental learning. In *AAAI*, 2025.

[36] Cédric Villani and Cédric Villani. The wasserstein distances. *Optimal transport: old and new*, 2009.

[37] C. Wah, S. Branson, P. Welinder, P. Perona, and S. Belongie. The Caltech-UCSD Birds-200-2011 Dataset. Technical Report CNS-TR-2011-001, California Institute of Technology, 2011.

[38] Fu-Yun Wang, Da-Wei Zhou, Han-Jia Ye, and De-Chuan Zhan. Foster: Feature boosting and compression for class-incremental learning. In *ECCV*, 2022.

[39] Liyuan Wang, Jingyi Xie, Xingxing Zhang, Mingyi Huang, Hang Su, and Jun Zhu. Hierarchical decomposition of prompt-based continual learning: Rethinking obscured sub-optimality. *NeurIPS*, 2023.

[40] Liyuan Wang, Jingyi Xie, Xingxing Zhang, Mingyi Huang, Hang Su, and Jun Zhu. Hierarchical decomposition of prompt-based continual learning: Rethinking obscured sub-optimality. In *NeurIPS*, 2023.

[41] Liyuan Wang, Jingyi Xie, Xingxing Zhang, Mingyi Huang, Hang Su, and Jun Zhu. Hierarchical decomposition of prompt-based continual learning: Rethinking obscured sub-optimality. *NeurIPS*, 2024.

[42] Liyuan Wang, Xingxing Zhang, Qian Li, Mingtian Zhang, Hang Su, Jun Zhu, and Yi Zhong. Incorporating neuro-inspired adaptability for continual learning in artificial intelligence. *Nature Machine Intelligence*, 2023.

[43] Liyuan Wang, Xingxing Zhang, Qian Li, Jun Zhu, and Yi Zhong. Coscl: Cooperation of small continual learners is stronger than a big one. In *ECCV*, 2022.

[44] Liyuan Wang, Xingxing Zhang, Hang Su, and Jun Zhu. A comprehensive survey of continual learning: Theory, method and application. *TPAMI*, 2024.

[45] Yabin Wang, Zhiheng Ma, Zhiwu Huang, Yaowei Wang, Zhou Su, and Xiaopeng Hong. Isolation and impartial aggregation: A paradigm of incremental learning without interference. In *AAAI*, 2023.

[46] Zhen Wang, Liu Liu, Yiqun Duan, and Dacheng Tao. Continual learning through retrieval and imagination. In *AAAI*, 2022.

[47] Zifeng Wang, Zizhao Zhang, Sayna Ebrahimi, Ruoxi Sun, Han Zhang, Chen-Yu Lee, Xiaoqi Ren, Guolong Su, Vincent Perot, Jennifer Dy, et al. Dualprompt: Complementary prompting for rehearsal-free continual learning. In *ECCV*, 2022.

[48] Zifeng Wang, Zizhao Zhang, Chen-Yu Lee, Han Zhang, Ruoxi Sun, Xiaoqi Ren, Guolong Su, Vincent Perot, Jennifer Dy, and Tomas Pfister. Learning to prompt for continual learning. In *CVPR*, 2022.

[49] Tongtong Wu, Xuekai Li, Yuan-Fang Li, Gholamreza Haffari, Guilin Qi, Yujin Zhu, and Guoqiang Xu. Curriculum-meta learning for order-robust continual relation extraction. In *AAAI*, 2021.

[50] Shipeng Yan, Jiangwei Xie, and Xuming He. Der: Dynamically expandable representation for class incremental learning. In *CVPR*, 2021.

[51] Bowen Zheng, Da-Wei Zhou, Han-Jia Ye, and De-Chuan Zhan. Task-agnostic guided feature expansion for class-incremental learning. *CVPR*, 2025.

[52] Zangwei Zheng, Mingyuan Ma, Kai Wang, Ziheng Qin, Xiangyu Yue, and Yang You. Preventing zero-shot transfer degradation in continual learning of vision-language models. In *ICCV*, 2023.

[53] Da-Wei Zhou, Zi-Wen Cai, Han-Jia Ye, De-Chuan Zhan, and Ziwei Liu. Revisiting class-incremental learning with pre-trained models: Generalizability and adaptivity are all you need. *IJCV*, 2024.

[54] Da-Wei Zhou, Hai-Long Sun, Jingyi Ning, Han-Jia Ye, and De-Chuan Zhan. Continual learning with pre-trained models: a survey. In *IJCAI*, 2024.

[55] Da-Wei Zhou, Hai-Long Sun, Han-Jia Ye, and De-Chuan Zhan. Expandable subspace ensemble for pre-trained model-based class-incremental learning. In *CVPR*, 2024.

[56] Da-Wei Zhou, Qi-Wei Wang, Han-Jia Ye, and De-Chuan Zhan. A model or 603 exemplars: Towards memory-efficient class-incremental learning. In *ICLR*, 2023.

[57] Da-Wei Zhou, Yuanhan Zhang, Yan Wang, Jingyi Ning, Han-Jia Ye, De-Chuan Zhan, and Ziwei Liu. Learning without forgetting for vision-language models. *TPAMI*, 2025.

[58] Kai Zhu, Wei Zhai, Yang Cao, Jiebo Luo, and Zheng-Jun Zha. Self-sustaining representation expansion for non-exemplar class-incremental learning. In *CVPR*, 2022.

Appendix

A Notation

Table A1 provides a detailed description of the notations used throughout the paper, facilitating a clearer understanding of the mathematical formulations and algorithmic procedures.

Table A1: Notations and their explanations used throughout this paper.

Notation	Explanation
N	Total number of classes.
$\mathcal{N}(\mu, \sigma^2)$	Gaussian (normal) distribution with mean μ and variance σ^2 .
\mathcal{D}^i	Training dataset for task i , consisting of n_i input–label pairs.
CLS^i	Set of classes associated with task i .
Ω	Sample space of all possible class sequences.
$\mathcal{O} \in \Omega$	A specific ordered class sequence of length K .
$\mathcal{P}_{\text{true}}$	True (but unknown) distribution of the model’s performance.
$\mathcal{A}(\mathcal{O})$	Final accuracy achieved by the model on sequence \mathcal{O} .
K	Total number of tasks (i.e., the length of each sequence).
L	Number of sampled sequences used for estimation.
δ	Allowed failure probability (so confidence is $1 - \delta$).
ϵ	Tolerance for estimation error.
$S(\mathcal{O})$	Inter-task similarity score for sequence \mathcal{O} .
ϵ_g	Theoretical upper bound on the generalization error.
Φ	CLIP text encoder mapping text tokens to d -dimensional embeddings.
\mathbf{L}	Matrix of text embeddings for the C class labels.
\mathbf{D}	Similarity matrix between label embeddings (e.g. cosine similarity).
ITS	Inter-task similarity matrix aggregated from \mathbf{D} .

B Detailed Analysis of RS Protocol

B.1 Theoretical Analysis and Proof

Lemma 1. *Let N be the total number of classes, partitioned into K tasks of equal size $M = N/K$. Then the number of distinct class sequences is $|\Omega| = \frac{N!}{(M!)^K}$. Moreover, under linear scaling $K = \Theta(N)$, the quantity $|\Omega|$ grows factorially, satisfying $|\Omega| = \Omega((N/e)^N)$, which asymptotically dwarfs any polynomial-scale sampling capacity as $N \rightarrow \infty$.*

Proof. We begin by noting that the total number of distinct permutations of N classes is $N!$. When partitioning these classes into K tasks of equal size $M = N/K$, each individual task contains M unordered classes. Since the order of classes within a task is irrelevant but the order of tasks themselves is preserved, we must quotient out the intra-task permutations.

For each task, there are $M!$ ways to permute its classes internally. Since there are K such tasks, the total number of intra-task permutations is $(M!)^K$. Consequently, the total number of distinct class sequences that respect this task-based structure is given by $|\Omega| = \frac{N!}{(M!)^K}$. To analyze the growth rate of $|\Omega|$, assume a linear scaling regime where $K = \Theta(N)$. Then $M = N/K = \Theta(1)$, implying that $M!$ is constant with respect to N . Therefore, $(M!)^K = \Theta(c^N)$ for some constant $c > 0$.

By Stirling’s approximation, we have:

$$N! \sim \sqrt{2\pi N} \left(\frac{N}{e} \right)^N. \quad (6)$$

Thus,

$$|\Omega| = \frac{N!}{(M!)^K} = \Omega \left(\frac{(N/e)^N}{c^N} \right) = \Omega \left(\left(\frac{N}{ec} \right)^N \right), \quad (7)$$

which shows that $|\Omega|$ grows at least as fast as $(N/e')^N$ for some constant $e' > e$, i.e., $|\Omega| = \Omega((N/e)^N)$.

Finally, note that any polynomial function in N is dominated by $(N/e)^N$ as $N \rightarrow \infty$. Hence, the number of possible class sequences $|\Omega|$ asymptotically exceeds any polynomial-scale sampling budget, concluding the proof. \square

Theorem 1. *Let Ω be the set of all possible class sequences with $|\Omega|$ elements, and fix tolerance $\varepsilon > 0$ and failure probability $\delta \in (0, 1)$. Suppose we draw L sequences $\{RS_l\}_{l=1}^L$ without replacement uniformly from Ω , and let $\widehat{\mathcal{A}}_L = \frac{1}{L} \sum_{l=1}^L \mathcal{A}(RS_l)$ be the empirical mean, respectively. Then for any $\varepsilon > 0$, if*

$$L \frac{|\Omega| - L}{|\Omega| - 1} \geq \frac{\ln(2|\Omega|/\delta)}{2\varepsilon^2}, \quad (8)$$

then with probability at least $1 - \delta$, $|\widehat{\mathcal{A}}_L - \mathbb{E}_\omega[\mathcal{A}(\omega)]| \leq \varepsilon$.

Proof. Let $\Omega = \{\omega_1, \omega_2, \dots, \omega_{|\Omega|}\}$ denote the finite set of all possible class sequences. Define the true mean accuracy as

$$\mu = \mathbb{E}_{\omega \sim \Omega}[\mathcal{A}(\omega)] = \frac{1}{|\Omega|} \sum_{i=1}^{|\Omega|} \mathcal{A}(\omega_i). \quad (9)$$

Let $\{RS_1, RS_2, \dots, RS_L\}$ be a sample of size L drawn uniformly at random *without replacement* from Ω , and define the empirical mean

$$\widehat{\mathcal{A}}_L = \frac{1}{L} \sum_{i=1}^L \mathcal{A}(RS_i). \quad (10)$$

Our goal is to bound the deviation probability $\mathbb{P}(|\widehat{\mathcal{A}}_L - \mu| \geq \varepsilon)$, under the assumption that $\mathcal{A}(\cdot) \in [0, 1]$ for all $\omega \in \Omega$. Let us define the Doob martingale sequence

$$Z_0 = \mathbb{E}[\widehat{\mathcal{A}}_L], \quad Z_i = \mathbb{E}[\widehat{\mathcal{A}}_L \mid RS_1, \dots, RS_i], \quad i = 1, \dots, L. \quad (11)$$

Then $\{Z_i\}_{i=0}^L$ forms a martingale with respect to the filtration $\mathcal{F}_i = \sigma(RS_1, \dots, RS_i)$, and we have:

$$Z_0 = \mu, \quad Z_L = \widehat{\mathcal{A}}_L, \quad \text{and} \quad \widehat{\mathcal{A}}_L - \mu = Z_L - Z_0 = \sum_{i=1}^L (Z_i - Z_{i-1}). \quad (12)$$

Since the sampling is without replacement from a bounded set $\mathcal{A}(\omega) \in [0, 1]$, we can bound each martingale difference:

$$|Z_i - Z_{i-1}| \leq \frac{1}{L} \cdot \sqrt{\frac{|\Omega| - L}{|\Omega| - 1}}, \quad \text{for all } i = 1, \dots, L. \quad (13)$$

This bound can be obtained via an extension of McDiarmid's inequality for sampling without replacement, or directly computed via sensitivity analysis of the sample mean with respect to one replacement in the sequence. Thus, the variance proxy is bounded as:

$$\sum_{i=1}^L (Z_i - Z_{i-1})^2 \leq L \cdot \left(\frac{1}{L^2} \cdot \frac{|\Omega| - L}{|\Omega| - 1} \right) = \frac{1}{L} \cdot \frac{|\Omega| - L}{|\Omega| - 1}. \quad (14)$$

Using the standard Azuma–Hoeffding inequality for martingales with bounded increments, we obtain:

$$\mathbb{P}(|\widehat{\mathcal{A}}_L - \mu| \geq \varepsilon) \leq 2 \exp \left(-\frac{\varepsilon^2}{2 \sum_{i=1}^L (Z_i - Z_{i-1})^2} \right) \leq 2 \exp \left(-2\varepsilon^2 L \cdot \frac{|\Omega| - L}{|\Omega| - 1} \right). \quad (15)$$

To ensure that the deviation probability is at most $\delta/|\Omega|$ for each of the $|\Omega|$ possible values (for use in a union bound), it suffices that:

$$2 \exp \left(-2\varepsilon^2 L \cdot \frac{|\Omega| - L}{|\Omega| - 1} \right) \leq \frac{\delta}{|\Omega|}. \quad (16)$$

Solving this inequality, we take logarithms on both sides:

$$-2\varepsilon^2 L \cdot \frac{|\Omega| - L}{|\Omega| - 1} \leq \ln(\delta/2S), \quad (17)$$

which is equivalent to:

$$L \cdot \frac{|\Omega| - L}{|\Omega| - 1} \geq \frac{\ln(2|\Omega|/\delta)}{2\varepsilon^2}. \quad (18)$$

□

Theorem 2. Let Ω be the set of all class sequences, and define $\mu = \mathbb{E}_{\omega \sim \Omega}[\mathcal{A}(\omega)]$, $\sigma = \sqrt{\text{Var}_{\omega \sim \Omega}[\mathcal{A}(\omega)]}$ as the realistic mean and standard deviation of the accuracy function \mathcal{A} . Suppose we know two extreme sequences ω_+ , ω_- satisfying $\mathcal{A}(\omega_+) - \mu \geq \sigma$ and $\mu - \mathcal{A}(\omega_-) \geq \sigma$. Draw L sequences $\{RS_i\}_{i=1}^L$ without replacement uniformly from $\Omega \setminus \{\omega_+, \omega_-\}$, and define $\tilde{\mathcal{A}}_{L+2} = \frac{1}{L+2} [\mathcal{A}(\omega_-) + \mathcal{A}(\omega_+) + \sum_{i=1}^L \mathcal{A}(RS_i)]$. Then for any $\varepsilon > 0$ and $\delta \in (0, 1)$, if

$$L \cdot \frac{|\Omega| - 2 - L}{|\Omega| - 3} \geq \frac{\ln(2(|\Omega| - 2)/\delta)}{2\varepsilon^2} (R^{(\sigma)})^2, \quad (19)$$

where $R^{(\sigma)} = \mathcal{A}(\omega_+) - \mathcal{A}(\omega_-)$, then with probability at least $1 - \delta$, $|\tilde{\mathcal{A}}_{L+2} - \mathbb{E}_{\omega \sim \Omega}[\mathcal{A}(\omega)]| \leq \varepsilon$.

Proof. Let $\Omega = \{\omega_1, \dots, \omega_{|\Omega|}\}$ and write

$$\mu = \frac{1}{|\Omega|} \sum_{i=1}^{|\Omega|} \mathcal{A}(\omega_i), \quad \sigma^2 = \text{Var}_{\omega \sim \Omega}[\mathcal{A}(\omega)] \quad (20)$$

By assumption there exist sequences ω_+ , ω_- satisfying

$$\mathcal{A}(\omega_+) - \mu \geq \sigma, \quad \mu - \mathcal{A}(\omega_-) \geq \sigma. \quad (21)$$

Define the total range

$$R^{(\sigma)} = \mathcal{A}(\omega_+) - \mathcal{A}(\omega_-) \geq 2\sigma. \quad (22)$$

Draw L samples $\{RS_i\}_{i=1}^L$ without replacement from $\Omega' = \Omega \setminus \{\omega_+, \omega_-\}$, and set

$$\tilde{\mathcal{A}}_{L+2} = \frac{1}{L+2} [\mathcal{A}(\omega_-) + \mathcal{A}(\omega_+) + \sum_{i=1}^L \mathcal{A}(RS_i)]. \quad (23)$$

Consider the Doob martingale

$$Z_0 = \mathbb{E}[\tilde{\mathcal{A}}_{L+2}], \quad Z_i = \mathbb{E}[\tilde{\mathcal{A}}_{L+2} \mid RS_1, \dots, RS_i], \quad i = 1, \dots, L. \quad (24)$$

Then

$$Z_0 = \mu, \quad Z_L = \tilde{\mathcal{A}}_{L+2}, \quad \tilde{\mathcal{A}}_{L+2} - \mu = \sum_{i=1}^L (Z_i - Z_{i-1}). \quad (25)$$

Since each $\mathcal{A}(RS_i)$ lies between the two extremes, replacing one sample can change the sum by at most $R^{(\sigma)}$. Moreover, because we sample without replacement from a set of size $|\Omega| - 2$, the sensitivity of the average $\tilde{\mathcal{A}}_{L+2}$ to a single replacement is further scaled by $\sqrt{(|\Omega| - 2 - L)/(|\Omega| - 3)}$. Altogether one obtains

$$|Z_i - Z_{i-1}| \leq \frac{1}{L+2} R^{(\sigma)} \sqrt{\frac{|\Omega| - 2 - L}{|\Omega| - 3}}, \quad i = 1, \dots, L. \quad (26)$$

Hence, the sum of squared increments is bounded by

$$\sum_{i=1}^L (Z_i - Z_{i-1})^2 \leq L \left(\frac{R^{(\sigma)}}{L+2} \right)^2 \frac{|\Omega| - 2 - L}{|\Omega| - 3}. \quad (27)$$

By Azuma–Hoeffding,

$$\Pr(|\tilde{\mathcal{A}}_{L+2} - \mu| \geq \varepsilon) \leq 2 \exp \left(-\frac{\varepsilon^2}{2 \sum_{i=1}^L (Z_i - Z_{i-1})^2} \right) \leq 2 \exp \left(-2\varepsilon^2 L \frac{|\Omega| - 2 - L}{|\Omega| - 3} (R^{(\sigma)})^{-2} \right). \quad (28)$$

Requiring this probability to be at most $\delta/(|\Omega| - 2)$ and solving for L gives

$$L \cdot \frac{|\Omega| - 2 - L}{|\Omega| - 3} \geq \frac{\ln(2(|\Omega| - 2)/\delta)}{2\varepsilon^2} (R^{(\sigma)})^2. \quad (29)$$

□

B.2 Empirical Analysis

To empirically validate the distributional characteristics of performance metrics across different continual learning methods, we conducted experiments on CIFAR-100 and ImageNet-R. As shown in Table A2, the number of possible class sequences grows rapidly even with a small number of classes. To balance feasibility and distributional richness, we chose a configuration with 6 classes divided into 3 tasks of 2 classes each, yielding 90 possible class sequences. This setting is large enough to exhibit meaningful variation in performance, yet still allows complete enumeration of the sequence space. For each dataset, we randomly selected 6 classes and partitioned them accordingly. We then evaluated two groups of methods:

Table A2: Number of possible class sequences $|\Omega|$ under different partitions

N	K	$M = N/K$	Formula	$ \Omega = \frac{N!}{(M!)^K}$
4	2	2	$\frac{4!}{(2!)^2}$	6
6	2	3	$\frac{6!}{(3!)^2}$	20
8	2	4	$\frac{8!}{(4!)^2}$	70
10	2	5	$\frac{10!}{(5!)^2}$	252
6	3	2	$\frac{6!}{(2!)^3}$	90
9	3	3	$\frac{9!}{(3!)^3}$	1680
8	4	2	$\frac{8!}{(2!)^4}$	2520

- **Non-pretrained CIL methods:** EWC [14], DER [50], iCaRL [29], FOSTER [38], MEMO [56], and TagFex [51].
- **Pre-trained CIL methods :** L2P [48], CODA-Prompt [33], HidePrompt [39], EASE [55], and MOS [35].

Observation 1: The capacity distribution of the model is near-Gaussian

For each method–dataset pair, we collected the final task accuracies over the 90 sequences and applied a Box–Cox power transformation. The optimal parameter λ was chosen by maximizing the log-likelihood under the normality assumption. We then performed three normality tests on the transformed accuracies: the Shapiro–Wilk test, D’Agostino’s K^2 test, and the one-sample Kolmogorov–Smirnov (KS) test. Each yields a p -value indicating the probability of observing the data under a Gaussian null hypothesis.

The results in Table A3 indicate that, after Box–Cox transformation, most method–dataset combinations exhibit p -values above the conventional 0.05 threshold in at least two of the three tests, suggesting an adequate approximation to normality.

In addition, methods not listed in Table A3, such as RanPAC and EASE, produce a limited number of possible task sequences due to their architectural design, resulting in insufficient sample sizes for reliable normality testing; hence, their results are reported as *n/a*.

Observation 2: The sampling of RS protocol cannot reflect the realistic ability of the model well

Figure A1 and Figure A2 illustrate the true performance distribution and the sampling locations obtained using the RS protocol (random seeds 0, 42, and 1993). Random sampling often fails to capture the true characteristics of the distribution. First, most sampled points cluster around the center of the distribution, making them ineffective in reflecting the model’s behavior under extreme conditions. Second, the randomness of the sampling process introduces significant uncertainty across different data types and datasets, as the sampling locations vary considerably. This variability leads to unstable evaluations, where some methods are overestimated while others are underestimated. Third, two major issues arise when using these randomly selected points to estimate the true distribution: the mean is inaccurately estimated, and the variance is severely underestimated. These problems together compromise the reliability of model evaluation under the RS protocol.

Observation 3: The performance of the model is positively correlated with inter-task similarity

Building upon the prior theoretical analysis and the first two observations, we recognize the necessity of incorporating extreme sequences for auxiliary evaluation. However, a key challenge lies in

Table A3: Normality test results after box–cox transformation, **demonstrating that the model capacity distribution approximates a Gaussian**

Method	Dataset	λ	Shapiro–Wilk p	D’Agostino’s p	KS p
CODA-Prompt	CIFAR-100	4.5971	0.4753	0.4357	0.8365
CODA-Prompt	ImageNet-R	2.3957	0.9321	0.7483	0.8811
DER	CIFAR-100	2.2577	0.3582	0.3030	0.3824
DER	ImageNet-R	0.0321	0.2755	0.5488	0.6937
EWC	CIFAR-100	1.5076	0.1926	0.1913	0.4064
EWC	ImageNet-R	0.7893	0.2854	0.5735	0.3519
FOSTER	CIFAR-100	2.8988	0.2215	0.9340	0.4010
FOSTER	ImageNet-R	0.1042	0.2216	0.1903	0.2880
Hide-Prompt	CIFAR-100	4.1164	0.5802	0.4904	0.4783
Hide-Prompt	ImageNet-R	1.7462	0.3538	0.8186	0.6373
iCaRL	CIFAR-100	7.2381	0.1369	0.0326	0.4413
iCaRL	ImageNet-R	1.1917	0.9577	0.9403	0.9870
L2P	CIFAR-100	11.8644	0.0554	0.3215	0.2628
L2P	ImageNet-R	4.4415	0.1850	0.1541	0.6715
MEMO	CIFAR-100	0.7041	0.1720	0.0524	0.7084
MEMO	ImageNet-R	0.6267	0.8781	0.8697	0.7357
MOS	CIFAR-100	-12.9763	0.4968	0.7681	0.5230
MOS	ImageNet-R	3.0909	0.1546	0.7973	0.2497

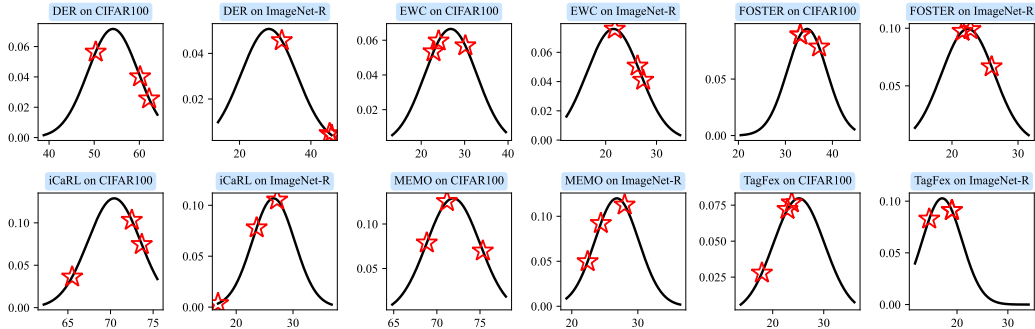


Figure A1: True performance distribution (black) and sampling positions under the RS protocol (blue) for non-pretrained CIL methods. The figure illustrates that RS fails to adequately capture the true distribution, leading to biased estimation.

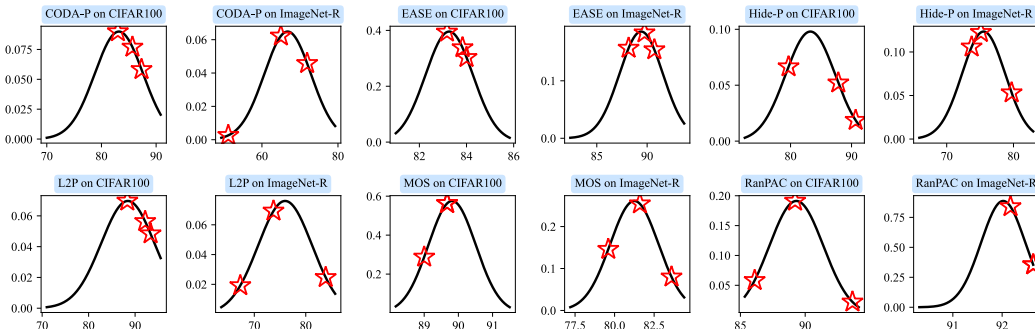


Figure A2: True data distribution and the sampling positions under the RS protocol (pre-trained CIL methods).

adaptively identifying such extreme sequences and determining a principled basis for algorithmic design. In the CIL setting, it is intuitively understood that when adjacent tasks exhibit low similarity,

the model parameters undergo substantial changes during task transitions, increasing the risk of forgetting. Motivated by this intuition, we investigate the relationship between inter-task similarity and model performance. As shown in Figure 2c, a strong positive correlation is observed across most methods. This insight suggests that inter-task similarity can be a foundation for designing strategies to sample challenging sequences and evaluate model robustness.

C Detailed Analysis of EDGE

C.1 Theoretical Analysis and Proof

Theorem 3. Consider a CIL system consisting of K tasks, where each task T_k is associated with a data distribution \mathcal{D}_k and a class set \mathcal{C}_k . The generalization error is defined as $\epsilon_g = \frac{1}{K} \sum_{k=1}^K \mathbb{E}_{(x,y) \sim \mathcal{D}_k} [L(h(x), y)]$, where $L(h(x), y)$ denotes the loss between the model prediction $h(x)$ and the true label y . Given a task order $\mathcal{O} = \{T_1, T_2, \dots, T_K\}$, the similarity score $\mathcal{S}(\mathcal{O})$ is defined as:

$$\mathcal{S}(\mathcal{O}) = \frac{K}{(K-1)N} \sum_{1 \leq i \leq K-1} \sum_{c \in \mathcal{C}_i} \sum_{c' \in \mathcal{C}_{i+1}} \text{Sim}(c, c'), \quad (30)$$

where $\text{Sim}(c, c')$ denotes the semantic similarity in the representation space between classes c and c' , belonging to tasks T_i and T_j , respectively. Let \mathcal{O}_h and \mathcal{O}_e denote the sequences with the minimum and maximum similarity scores $\mathcal{S}(\mathcal{O})$, respectively, and let \mathcal{O}_r represent a randomly generated sequence. Then, the following conditions hold:

- The similarity score satisfies $\mathcal{S}(\mathcal{O}_h) \leq \mathcal{S}(\mathcal{O}_r) \leq \mathcal{S}(\mathcal{O}_e)$,
- The generalization error satisfy $\epsilon_g(\mathcal{O}_h) \geq \epsilon_g(\mathcal{O}_r) \geq \epsilon_g(\mathcal{O}_e)$.

Lemma 2. [21] When $p \geq n + 2$, we must have:

$$\begin{aligned} \mathbb{E}[\epsilon_g] &= \frac{r^T}{T} \sum_{i=1}^{T-1} \|w_i^*\|^2 + \frac{1-r}{T} \sum_{i=1}^T r^{T-i} \sum_{k=1}^T \|w_k^* - w_i^*\|^2 \\ &\quad + \frac{p\sigma^2}{p-n-1} (1-r^T). \end{aligned} \quad (31)$$

where the overparameterization ratio $r = 1 - \frac{n}{p}$ in this context quantifies the degree of overparameterization in a model, where n represents the sample size, and p denotes the number of model parameters. The coefficients $c_{i,j} = (1-r)(r^{T-i} - r^{j-i} + r^{T-j})$, with $1 \leq i < j \leq T$, correspond to the indices of tasks, and σ denotes a coefficient representing the model's noise level.

Proof. First, consider the total cross-task similarity:

$$\sum_{1 \leq i \leq K} \sum_{1 \leq j \leq K} \sum_{c \in \mathcal{C}_i} \sum_{c' \in \mathcal{C}_j} \text{Sim}(c, c'), \quad (32)$$

and the intra-task similarity:

$$\sum_{1 \leq i \leq K} \sum_{c, c' \in \mathcal{C}_i} \text{Sim}(c, c'). \quad (33)$$

These satisfy the conservation relationship:

$$\sum_{1 \leq i \leq K} \sum_{1 \leq j \leq K} \sum_{c \in \mathcal{C}_i} \sum_{c' \in \mathcal{C}_j} \text{Sim}(c, c') + \sum_{1 \leq i \leq K} \sum_{c, c' \in \mathcal{C}_i} \text{Sim}(c, c') = C_1. \quad (34)$$

For optimal parameters between tasks i and j , we have:

$$\begin{aligned} \|w_i^* - w_j^*\|^2 &\propto \left\| \sum_{m \in \mathcal{C}_i} v_m^* - \sum_{n \in \mathcal{C}_j} v_n^* \right\|^2 \\ &= \sum_{m \in \mathcal{C}_i} \sum_{n \in \mathcal{C}_j} \langle v_m, v_n \rangle + \sum_{m \in \mathcal{C}_j} \sum_{n \in \mathcal{C}_i} \langle v_m, v_n \rangle - 2 \sum_{m \in \mathcal{C}_i} \sum_{n \in \mathcal{C}_j} \langle v_m, v_n \rangle \end{aligned}$$

$$= \alpha \left(\sum_{c, c' \in \mathcal{C}_i} \text{Sim}(c, c') + \sum_{c, c' \in \mathcal{C}_j} \text{Sim}(c, c') \right) - \alpha \sum_{c \in \mathcal{C}_i} \sum_{c' \in \mathcal{C}_j} \text{Sim}(c, c'), \quad (35)$$

where α is a proportionality constant.

Substituting into the key term from Lemma 2:

$$\begin{aligned} & \frac{1-r}{K} \sum_{i=1}^K r^{K-i} \sum_{k=1}^K \|w_k^* - w_i^*\|^2 \\ &= \frac{1-r}{K} \sum_{i=1}^K r^{K-i} \sum_{k=1}^K \alpha \left(\sum_{c, c' \in \mathcal{C}_i} \text{Sim}(c, c') + \sum_{c, c' \in \mathcal{C}_k} \text{Sim}(c, c') - \sum_{c \in \mathcal{C}_i} \sum_{c' \in \mathcal{C}_k} \text{Sim}(c, c') \right) \\ &= \frac{1-r}{K} \sum_{i=1}^K r^{K-i} \alpha \left((K-1) \sum_{c, c' \in \mathcal{C}_i} \text{Sim}(c, c') - \sum_{k=1}^K \sum_{c \in \mathcal{C}_i} \sum_{c' \in \mathcal{C}_k} \text{Sim}(c, c') \right) \\ &= \frac{1-r^K}{K} \alpha (K-1) \left(C_1 - \sum_{i=1}^K \sum_{j=1, j \neq i}^K \sum_{c \in \mathcal{C}_i} \sum_{c' \in \mathcal{C}_j} \text{Sim}(c, c') \right) \\ &\quad - \frac{1-r}{K} \sum_{i=1}^K r^{K-i} \alpha \sum_{k=1}^K \sum_{c \in \mathcal{C}_i} \sum_{c' \in \mathcal{C}_k} \text{Sim}(c, c') \\ &= (1-r^K) \alpha C_1 - \frac{1-r}{K} \alpha \sum_{i=1}^K \sum_{k=1, k \neq i}^K r^{k-i} \sum_{c \in \mathcal{C}_i} \sum_{c' \in \mathcal{C}_k} \text{Sim}(c, c') \\ &= C_2 - 2 \frac{r-r^2}{K} \alpha \sum_{1 \leq i \leq K-1} \sum_{c \in \mathcal{C}_i} \sum_{c' \in \mathcal{C}_{i+1}} \text{Sim}(c, c'), \end{aligned} \quad (36)$$

where C_2 contains terms independent of the task ordering.

To establish the probabilistic bound for random sequences, let Ω denote the set of all possible task permutations and $\mathcal{O}_r \sim \text{Unif}(\Omega)$. Define the random variable $X_{i,j} = \sum_{c \in \mathcal{C}_i} \sum_{c' \in \mathcal{C}_j} \text{Sim}(c, c')$. The similarity score can be rewritten as:

$$\mathcal{S}(\mathcal{O}) = \frac{K}{(K-1)N} \sum_{t=1}^{K-1} X_{\pi(t), \pi(t+1)}, \quad (37)$$

where π is the permutation function. By symmetry, the probability that any two distinct tasks T_i and T_j are adjacent in a random permutation is $\frac{2}{K(K-1)}$. Thus, the expected similarity score is:

$$\begin{aligned} \mathbb{E}[\mathcal{S}(\mathcal{O}_r)] &= \frac{K}{(K-1)N} \cdot \frac{2}{K(K-1)} \sum_{1 \leq i < j \leq K} X_{i,j} \\ &= \frac{2}{(K-1)^2 N} \sum_{i \neq j} X_{i,j}. \end{aligned} \quad (38)$$

Applying McDiarmid's inequality to the function $f(\pi) = \mathcal{S}(\mathcal{O})$, observe that swapping two tasks in π changes $f(\pi)$ by at most $\frac{4U}{N}$, where U is the upper bound of $\text{Sim}(c, c')$. This yields:

$$\mathbb{P}(|f(\pi) - \mathbb{E}[f]| \geq \delta) \leq 2 \exp \left(-\frac{2\delta^2 N^2}{K(4U)^2} \right). \quad (39)$$

Letting $\delta = \min(\mathbb{E}[f] - \mathcal{S}(\mathcal{O}_h), \mathcal{S}(\mathcal{O}_e) - \mathbb{E}[f])$, we obtain the concentration bound:

$$\mathbb{P}(\mathcal{S}(\mathcal{O}_h) \leq \mathcal{S}(\mathcal{O}_r) \leq \mathcal{S}(\mathcal{O}_e)) \geq 1 - 2 \exp \left(-\frac{K\delta^2}{8U^2} \right). \quad (40)$$

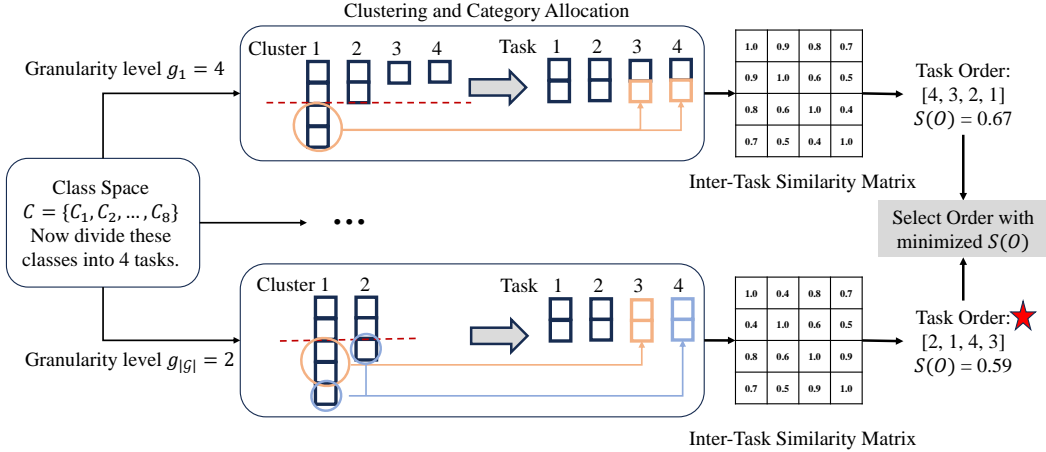


Figure A3: Details of generating difficult category sequences (Algorithm 1)

This reveals an inverse relationship between the similarity score $S(\mathcal{O})$ and the generalization error ϵ_g : the coefficient before the similarity summation term is negative, meaning higher similarity scores correspond to lower generalization error. Therefore, the ordering with maximum similarity \mathcal{O}_e minimizes ϵ_g , while the minimum similarity ordering \mathcal{O}_h maximizes ϵ_g , with random ordering \mathcal{O}_r falling between them. \square

C.2 Pseudo Code and Analysis

Algorithm 1 Hard Task Sequence Generation Algorithm

Require: Similarity matrix \mathbf{D} , classes number N , tasks number K , candidate granularities set \mathcal{G}
Ensure: Task sequence \mathcal{O}

- 1: Initialize similarity graph $G \leftarrow \mathbf{D}$; set $G_{ii} \leftarrow 0$ for all i
- 2: Compute dissimilarity matrix $M \leftarrow \mathbf{I} - G$
- 3: **for** Granularity level $g \in \mathcal{G}$ **do**
- 4: Perform hierarchical clustering on M into g clusters
- 5: Merge clusters into K tasks $\{\mathcal{C}_1, \dots, \mathcal{C}_K\}$, minimizing cross-cluster task assignment
- 6: Initialize inter-task similarity matrix $\mathbf{ITS} \in \mathbb{R}^{K \times K}$
- 7: **for** $i, j \in [K]$, $i \neq j$ **do**
- 8: $\mathbf{ITS}_{ij} \leftarrow \frac{1}{|\mathcal{C}_i||\mathcal{C}_j|} \sum_{c_1 \in \mathcal{C}_i} \sum_{c_2 \in \mathcal{C}_j} G_{c_1 c_2}$
- 9: **end for**
- 10: Select the first task: $\mathcal{O}_g \leftarrow [\arg \min_{k \in [K]} \sum_{j \in [K], j \neq k} \mathbf{ITS}_{kj}]$
- 11: Initialize remaining task set: $\mathcal{R} \leftarrow [K] \setminus \mathcal{O}_g$
- 12: **while** $\mathcal{R} \neq \emptyset$ **do**
- 13: Select the next task: $k^* \leftarrow \arg \min_{k \in \mathcal{R}} \sum_{t \in \mathcal{O}_g} \mathbf{ITS}_{tk}$
- 14: Append k^* to the task sequence: $\mathcal{O}_g \leftarrow \mathcal{O}_g \circ k^*$
- 15: Update remaining task set: $\mathcal{R} \leftarrow \mathcal{R} \setminus \{k^*\}$
- 16: **end while**
- 17: Compute sequence score $S(\mathcal{O}_g)$ according to Equation (30)
- 18: **end for**
- 19: Select the sequence: $\mathcal{O} \leftarrow \arg \min_{\mathcal{O}_g} S(\mathcal{O}_g)$
- 20: **return** \mathcal{O}

Algorithm Analysis. The proposed algorithm generates hard task sequences by systematically minimizing inter-task similarities, which aligns with Theorem 1's conclusion that lower similarity scores correspond to higher generalization error. Key design rationales are analyzed as follows:

- **Step 2-3 (Dissimilarity Computation):** First, we convert the class similarity matrix $\mathbf{G} \in \mathbb{R}^{N \times N}$ into a dissimilarity matrix by computing $\mathbf{D} = \mathbf{1} - \mathbf{G}$ and setting the diagonal to zero. This

transformation ensures compatibility with clustering algorithms, where larger values indicate greater dissimilarity. Next, we apply hierarchical clustering with complete linkage on the condensed form of \mathbf{D} to obtain K clusters. These clusters are then sorted by size in descending order. For clusters whose size exceeds the base task size $M = N/K$, we iteratively assign subsets of the cluster to the currently smallest task to preserve internal semantic similarity while maintaining balance. For smaller clusters, we assign all classes directly to the current shortest task. After this initial allocation, we perform a final adjustment step to ensure all tasks are of equal size: any task exceeding the base size has its excess classes redistributed to tasks with fewer classes. This process results in K balanced tasks, each composed of semantically coherent classes, effectively minimizing global inter-task similarity and supporting the construction of hard class sequences.

- **Step 4-5 (Multi-Granularity Clustering):** Varying granularity levels $g \in \mathcal{G}$ enable exploration of different class grouping resolutions. This multi-scale approach increases the probability of discovering optimal task boundaries that minimize cross-task similarities.
- **Step 6-9 (Inter-Task Similarity Matrix):** The normalized average similarity ITS_{ij} accurately reflects task relationships as defined in Equation (30). This ensures algorithmic objectives align with theoretical similarity metrics.
- **Step 10-16 (Greedy Sequence Construction):** The initialization strategy selects the most isolated task as the starting point, preventing early error propagation. The iterative selection of least similar subsequent tasks implements a locally optimal strategy that approximates global minimization of $\mathcal{S}(\mathcal{O})$.
- **Step 17 (Multi-Granularity Optimization):** Evaluating multiple granularities leverages Equation (30), where better local minima are more likely to be found through diversified grouping strategies.

Figure A3 provides an illustrative example of the proposed procedure. Suppose we are given 8 classes to be partitioned into 4 tasks. Under a finer clustering granularity, the classes are grouped into 4 clusters, where the first cluster contains 4 classes, the second contains 3, and the remaining two contain 1 class each. To maintain high intra-task similarity, the two extra classes in the first cluster are redistributed to clusters 3 and 4, resulting in a balanced 4-task partition.

Under a coarser granularity, the same 8 classes might be clustered into only 2 groups: the first cluster with 5 classes and the second with 3. In this case, two of the most semantically similar classes from the larger cluster are assigned to form a new task, while the remaining two form another task, resulting in 4 tasks overall.

After generating task partitions, we compute the Inter-Task Similarity (ITS) matrix and select an initial task with the lowest global similarity. We then construct candidate sequences by greedily adding tasks with the smallest pairwise similarity to the most recently added task. For example, from this procedure, we may derive two sequences: $4 \rightarrow 3 \rightarrow 2 \rightarrow 1$ and $2 \rightarrow 1 \rightarrow 4 \rightarrow 3$, with corresponding similarity scores of 0.67 and 0.59, respectively. This process is repeated across clustering granularities, and the sequence with the lowest overall similarity score $\mathcal{S}(\mathcal{O})$ is ultimately selected as the hard sequence.

Theorem 4 (Greedy Strategy Optimality Bound). *Let \mathcal{O}_r be a uniformly random permutation of K tasks and define the average inter-task similarity*

$$\bar{S} = \frac{1}{\binom{K}{2}} \sum_{1 \leq i < j \leq K} \frac{1}{|\mathcal{C}_i| |\mathcal{C}_j|} \sum_{c \in \mathcal{C}_i} \sum_{c' \in \mathcal{C}_j} \text{Sim}(c, c'), \quad (41)$$

and assume $0 \leq \text{Sim}(c, c') \leq U$. Let \mathcal{O}_g be the sequence produced by the greedy Algorithm 1. Then with probability at least $1 - e^{-K/2}$,

$$\mathcal{S}(\mathcal{O}_g) \leq \mathbb{E}[\mathcal{S}(\mathcal{O}_r)] - \Delta, \quad (42)$$

where

$$\mathbb{E}[\mathcal{S}(\mathcal{O}_r)] = \frac{N^2 (K-1)}{2K^2} \bar{S}, \quad \Delta = \frac{N^2 (K-1)}{2K^2} \bar{S} - \frac{2N (\ln K + 1)}{K-1} U. \quad (43)$$

In particular, if $\bar{S} \geq \frac{4K^2 (\ln K + 1)}{N(K-1)^2} U$, then $\Delta > 0$ and hence $\mathcal{S}(\mathcal{O}_g) < \mathbb{E}[\mathcal{S}(\mathcal{O}_r)]$.

Proof. Define, for $i < j$,

$$X_{i,j} = \sum_{c \in \mathcal{C}_i} \sum_{c' \in \mathcal{C}_j} \text{Sim}(c, c'). \quad (44)$$

Since each pair (i, j) appears adjacent with probability $\frac{2}{K(K-1)}$,

$$\mathbb{E}[\mathcal{S}(\mathcal{O}_r)] = \sum_{i < j} \frac{2}{K(K-1)} X_{i,j} = \frac{2}{K(K-1)} \sum_{i < j} X_{i,j}. \quad (45)$$

Noting $|\mathcal{C}_i| = N/K$, one finds

$$\sum_{i < j} X_{i,j} = \binom{K}{2} \frac{N^2}{K^2} \bar{S} \implies \mathbb{E}[\mathcal{S}(\mathcal{O}_r)] = \frac{N^2(K-1)}{2K^2} \bar{S}. \quad (46)$$

At step t of Algorithm 1, there are $t(K-t)$ candidate edges, each bounded by N^2U . By standard order-statistic arguments,

$$\mathbb{E}[\Delta_t] \leq \frac{N^2U}{t(K-t)+1}, \quad (47)$$

and a union bound shows that with probability $\geq 1 - e^{-K/2}$ each Δ_t is at most twice its mean. Summing over $t = 1, \dots, K-1$ gives

$$\mathbb{E}[\mathcal{S}(\mathcal{O}_g)] \leq \frac{K}{(K-1)N} \sum_{t=1}^{K-1} \frac{N^2U}{t(K-t)+1} \leq \frac{2N(\ln K + 1)}{K-1} U. \quad (48)$$

With probability at least $1 - e^{-K/2}$,

$$\mathcal{S}(\mathcal{O}_g) \leq 2\mathbb{E}[\mathcal{S}(\mathcal{O}_g)] \leq \frac{4N(\ln K + 1)}{K-1} U. \quad (49)$$

Therefore

$$\mathbb{E}[\mathcal{S}(\mathcal{O}_r)] - \mathcal{S}(\mathcal{O}_g) \geq \frac{N^2(K-1)}{2K^2} \bar{S} - \frac{4N(\ln K + 1)}{K-1} U = \Delta, \quad (50)$$

Completing the proof. \square

Theorem 4 tells us that the greedy strategy of always choosing the most similar remaining pair of tasks takes advantage of strong inter-task affinities to produce an ordering whose total similarity remains tightly controlled and, when the average similarity is high enough, is lower than that of a random arrangement. The theorem shows that optimal local choices based only on current similarity scores accumulate into a reliable global solution even in noise.

Complexity Analysis. With a time complexity of $O(|\mathcal{G}|(N^3 + K^3))$, the algorithm remains tractable for practical CIL scenarios where $K \ll N$. The cubic terms stem primarily from hierarchical clustering (Step 4) and inter-task similarity computations (Step 6–9). In practice, these steps can be further accelerated using approximate nearest neighbor techniques. For instance, when partitioning 100 classes into 10 tasks, the algorithm completes in approximately **0.5 seconds**; for 200 classes into 10 tasks, it takes around **0.9 seconds** on a standard CPU, demonstrating its efficiency for common CIL settings.

Similarly, Algorithm 2 presents the pseudocode for constructing a simple task sequence by iteratively selecting and appending each task according to the prescribed rule.

D Detailed Analysis of Experiment

D.1 Enumerable Experiments

D.1.1 Experimental setup

Dataset and Metrics. We conduct experiments on two standard benchmarks: CIFAR-100 [15] and ImageNet-R [15]. For each, we select the first six semantic classes and group them into three

Algorithm 2 Easy Task Sequence Generation Algorithm

Require: Similarity matrix \mathbf{D} , classes number N , tasks number K , candidate granularities set \mathcal{G}
Ensure: Task sequence \mathcal{O}

- 1: Initialize similarity graph $G \leftarrow I - \mathbf{D}$; set $G_{ii} \leftarrow 0$ for all i
- 2: Compute dissimilarity matrix $M \leftarrow \mathbf{I} - G$
- 3: **for** Granularity level $g \in \mathcal{G}$ **do**
- 4: Perform hierarchical clustering on M into g clusters
- 5: Merge clusters into K tasks $\{\mathcal{C}_1, \dots, \mathcal{C}_K\}$, minimizing cross-cluster task assignment
- 6: Initialize inter-task similarity matrix $\mathbf{ITS} \in \mathbb{R}^{K \times K}$
- 7: **for** $i, j \in [K], i \neq j$ **do**
- 8: $\mathbf{ITS}_{ij} \leftarrow \frac{1}{|\mathcal{C}_i||\mathcal{C}_j|} \sum_{c_1 \in \mathcal{C}_i} \sum_{c_2 \in \mathcal{C}_j} G_{c_1 c_2}$
- 9: **end for**
- 10: Select the first task: $\mathcal{O}_g \leftarrow [\arg \max_{k \in [K]} \sum_{j \in [K], j \neq k} \mathbf{ITS}_{kj}]$
- 11: Initialize remaining task set: $\mathcal{R} \leftarrow [K] \setminus \mathcal{O}_g$
- 12: **while** $\mathcal{R} \neq \emptyset$ **do**
- 13: Select the next task: $k^* \leftarrow \arg \max_{k \in \mathcal{R}} \sum_{t \in \mathcal{O}_g} \mathbf{ITS}_{tk}$
- 14: Append k^* to the task sequence: $\mathcal{O}_g \leftarrow \mathcal{O}_g \circ k^*$
- 15: Update remaining task set: $\mathcal{R} \leftarrow \mathcal{R} \setminus \{k^*\}$
- 16: **end while**
- 17: Compute sequence score $\mathcal{S}(\mathcal{O}_g)$ according to Equation (30)
- 18: **end for**
- 19: Select the sequence: $\mathcal{O} \leftarrow \arg \max_{\mathcal{O}_g} \mathcal{S}(\mathcal{O}_g)$
- 20: **return** \mathcal{O}

sequential learning tasks of two classes each, yielding a total of $3! = 6$ possible task orders per dataset; by considering all class-to-task assignments, we obtain 90 distinct sequences, which we treat as the ground-truth distribution $\mathcal{D}_{\text{true}}$. To estimate this distribution in practice, we use:

- **Random Seed (RS) protocol:** draw task sequences by shuffling class-labels under random seeds $\{0, 42, 1993\}$ [16, 18, 24, 48], forming the empirical distribution \mathcal{D}_{RS} .
- **EDGE protocol:** apply our edge-selection strategy on the same seeds to produce $\mathcal{D}_{\text{EDGE}}$.

We compare each estimated distribution to $\mathcal{D}_{\text{true}}$ using two complementary divergence metrics:

- **Jensen–Shannon divergence JSD_d :** Given two discrete distributions P and Q over the same support, the Jensen–Shannon divergence is defined as

$$JSD(P \parallel Q) = \frac{1}{2} D_{\text{KL}}(P \parallel M) + \frac{1}{2} D_{\text{KL}}(Q \parallel M), \quad M = \frac{1}{2}(P + Q),$$

where D_{KL} is the Kullback–Leibler divergence. Unlike D_{KL} , the JSD is symmetric and bounded in $[0, \ln 2]$, which makes it well suited for measuring similarity between empirical distributions with potentially non-overlapping support [17].

- **Wasserstein distance W_d :** Also known as the Earth Mover’s Distance, the first-order Wasserstein distance between P and Q on a metric space (\mathcal{X}, d) is

$$W_1(P, Q) = \inf_{\gamma \in \Gamma(P, Q)} \mathbb{E}_{(x, y) \sim \gamma} [d(x, y)],$$

where $\Gamma(P, Q)$ denotes the set of all joint distributions with marginals P and Q . In the discrete case, this reduces to the minimum cost of transporting “mass” from P to Q , providing a meaningful measure of distributional distance that accounts for the geometry of the task-permutation space [36].

Implementation Details. All methods are implemented in PyTorch with the following shared hyperparameters:

- **Memory:** total size 2000, up to 20 samples per class, non-fixed allocation.
- **Backbone:** ResNet-18, trained from scratch in the non-pre-trained setting and with ImageNet pre-training otherwise.

- **Optimizer & Scheduler:** SGD with step-LR; initial learning rate 0.1, weight decay 5×10^{-4} , LR decay factor 0.1 at epochs $\{60, 120, 170\}$ (non-pre-trained) or $\{80, 120, 150\}$ (pre-trained).
- **Training:** 170 epochs, batch size 128.

D.1.2 Additional Experiment Results

Table A4: Fitting performance of EDGE on CIFAR-100 using HidePrompt with various backbones. **EDGE consistently outperforms RS across nearly all backbones, demonstrating its effectiveness and robustness to different model architectures.**

Model	JSD_d	W_d
RS Estimate	0.2694	2.8688
EDGE with ResNet50	0.0863	1.5677
EDGE with ResNet50 \times 64	0.1986	3.2553
EDGE with ResNet101	0.1386	1.7020
EDGE with ViT-B/16	0.1236	1.5196
EDGE with ViT-B/32	0.1237	2.3599
EDGE with ViT-L/14	0.0846	1.0642

Table A4 summarizes the fitting performance of the EDGE method on the CIFAR-100 dataset under the HidePrompt setting, using various backbone architectures. The performance is evaluated in terms of Jensen-Shannon Divergence (JSD_d) and the 2-Wasserstein distance (W_d). Among all configurations, EDGE with ViT-L/14 best fits the reference distribution, yielding the lowest JSD_d (0.0846 bits) and the smallest W_d distance (1.0642).